

All-optical generation and photoassociative probing of sodium Bose-Einstein condensates

R. Dume, M. Johannig, E. Gombez, J. D. Einstein, K. M. Jones and P. D. Lett
 Atom Physics Division, National Institute of Standards and Technology, Gaithersburg, MD 20899-8424
 (Dated: February 5, 2020)

We demonstrate an all-optical technique to evaporatively produce sodium Bose-Einstein condensates (BEC). We use a crossed-dipole trap formed from light near 1 m, and a simple ramp of the intensity to force evaporation. In addition, we introduce photoassociation as diagnostic of the trap loading process, and show that it can be used to detect the onset of Bose-Einstein condensation. Finally, we demonstrate the straightforward production of multiple traps with condensates using this technique, and that some control over the spinor state of the BEC is achieved by positioning the trap as well.

PACS numbers: 03.75.Hh, 03.75.Be, 32.80.Pj, 39.20.+q

I. INTRODUCTION

All-optical approaches to attaining Bose-Einstein condensation (BEC) allow the trapping of spin-zero species (which cannot be held in a magnetic trap), and multiple, arbitrary spin states at once. In addition, the technique is convenient, avoiding large magnetic field coils that restrict optical access and allowing rapid evaporative cooling and condensation. A number of variations on this technique have been used successfully to condense a variety of atomic species. Here we present the first all-optical approach to evaporatively obtain BEC in sodium. Additionally, we extend the technique to multiple traps in a configuration useful for atom optics experiments. Our stainless steel vacuum chamber incorporates an ion detector which we use to sensitively detect photoassociation transitions. This signal is sensitive to the atomic density and provides a convenient way to optimize the loading of our dipole trap and BEC formation within the trap.

The first demonstration of evaporative cooling of a sodium gas held in a crossed dipole trap [1] was performed in 1995. The trap was formed by a pair of beams from a Nd:YAG laser operating at 1.06 m, detuned well red of the atomic resonance. In these studies the phase space density of the gas was increased by a factor of 28, but did not reach the conditions required to Bose-condense the rather small sample used. Later that year BEC in sodium was first observed [2] in a trap that employed magnetic confinement along with an optical "plug" to keep atoms away from a region of zero magnetic field. While magnetic traps of many forms have since dominated BEC studies, interest in all-optical methods has continued as well.

In this paper we return to investigate evaporative cooling of sodium in a crossed-beam dipole trap. With sufficient initial loading of the dipole trap, we find that it is relatively straightforward to achieve BEC with up to 2.5×10^5 ^{23}Na atoms by simply ramping down the trap laser intensity. The dipole trapping beams give us flexibility in arranging the location of the condensate and allows us to create traps with different spin-component

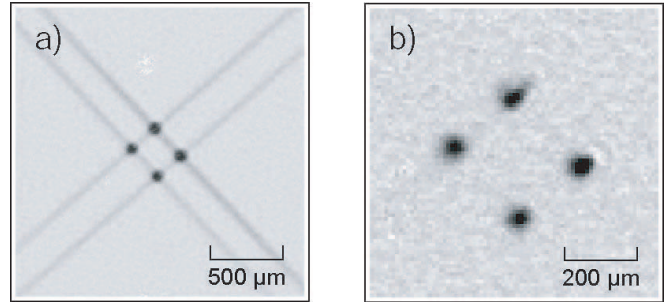


FIG. 1: a) Absorption image of four crossed dipole traps taken just after loading from a magneto-optical trap. This array was generated by recycling the trapping beams. The traps have a separation of 250 m. Atoms loaded into the arms of the trap make them visible before evaporation. b) Absorption image of the traps taken after evaporation, as described in the text, showing four BEC's.

populations. By recycling the beams, we construct multiple crossing regions with variable spacings. For instance, we can easily arrange a square array of four optical traps, spaced by 250 m, and produce a condensate in each trap, as shown in Fig. 1. Such arrays of condensates can be useful in a number of atom optics and fundamental physics experiments.

II. BACKGROUND

Producing BEC without the use of a magnetic trap was first demonstrated with ^{87}Rb in 2001 [3]. In this experiment the trap was formed by crossed, tightly-focussed beams from a CO₂ laser operating at a wavelength near 10 m. Since that time BEC in optical traps has been observed with several other species as well, using traps and procedures of varying complexity. ^{133}Cs [4] was condensed in a combined CO₂/fiber laser dipole trap. Cs is heavy and difficult to condense, requiring magnetic field gradients to cancel the force of gravity and bias fields to tune the scattering length by using a magnetic Fesh-

bach resonance. In this case weakly-focussed beams from the CO_2 -laser trap the Cs atoms, and a tightly-focussed beam at 1064 nm is introduced to create a "dimple" in the trap, where atoms can evaporate to higher density. Cr was recently condensed [5] by an evaporative cooling sequence which begins in a magnetic trap, and is completed after transferring the atoms to a crossed-dipole optical trap. Such traps are not restricted to the infrared: ^{174}Yb , with its strongest transition near 400 nm, was condensed in a crossed-dipole trap [6] formed from a 532 nm laser. The technique is also applicable to fermions, and evaporative cooling in a single beam CO_2 -laser optical trap has also been used to produce a degenerate Fermi gas of ^6Li atoms [7].

Many variations of the loading sequence, including the ramping of laser intensity and magnetic field, as well as dynamical changes in the optical system, have proven successful. Many of these complexities are dictated by the species of the atomic species that are used, especially their collision properties. In comparison with many of these previous experiments, sodium BEC can be achieved in a relatively simple sequence. No magnetic field gradient is required to compensate for gravity, and we use 1.07 m light from a fiber laser, which does not require the special window materials that are needed in the far infrared. Furthermore, we use a simple intensity ramp with no moving optics, resulting in a relatively uncomplicated and robust procedure.

We begin our experiment with atoms accumulated in a magneto-optical trap (MOT) fed with a zero-crossing Zeeman slower. Our MOT is of order 2 mm in diameter, while the optical trap has a $1/e^2$ waist of 61×3 m, resulting in a poor geometric overlap for loading. As discussed in Ref. [8] the loading process is somewhat complex and various schemes have been developed for improving it. To attain BEC in our experiments we have maintained a fixed trap size and concentrated on optimizing the loading by adjusting the way in which we ramp down the MOT light and magnetic field.

To monitor the buildup of the atomic density in the optical trap we introduce a photoassociation technique. Photoassociation (PA) is the process where two colliding atoms absorb a photon and form an electronically excited diatomic molecule [9, 10] (see Fig. 2). Photoassociation has been used to produce high-resolution spectra of the molecular states that are accessible in this way. The photoassociation transition can be detected in a number of ways, the two most common are trap loss and ionization. When a molecule is formed two atoms are removed from the trap, and a simple detection of atom number (by absorption or fluorescence), as a function of frequency, can be used to locate a PA transition. If the excited molecule can be further excited to an autoionizing state, or to an ionization continuum, the presence of an ion signal will indicate the PA transition. On the other hand, the technique can also be used as a probe for a number of effects, such as wavefunction distortion by magnetic [11] or optical-Feshbach [12] resonances, or, as in this case, as a sen-

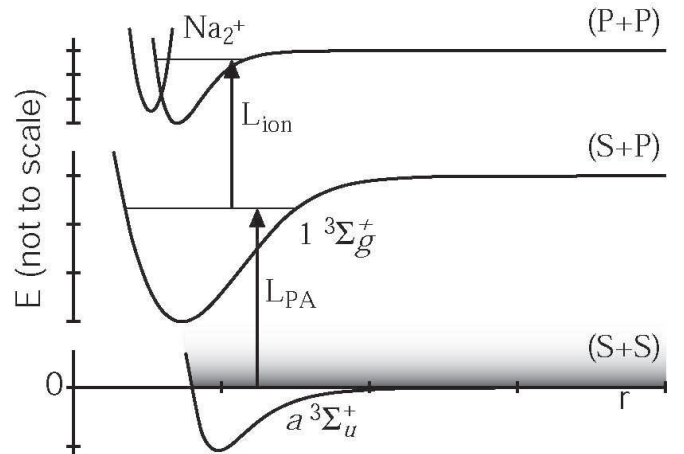


FIG. 2: Sketch of the relevant Na_2 molecular potentials and coupling lasers. The photoassociation laser L_{PA} couples colliding atoms with energy E to form an excited-state molecule. The excited state is resonantly excited to an autoionizing state by L_{ion} , resulting in an ion signal proportional to the excited state population.

sitive probe of the atomic density. Many of the low-lying states of Na_2 have been studied using photoassociation techniques, and in the current experiments we take advantage of a photoassociation-ionization transition that we have used in previous spectroscopy experiments [13].

We demonstrate that we can monitor the evolution of the trap density in our experiment using a PA ionization signal produced by two auxiliary lasers. One laser is tuned to a known molecular transition and the second is tuned to promote the excited molecule to a high-lying autoionizing state. The result is the production of Na_2^+ ions, which we detect with a microchannel plate. For the present purposes the important feature of the PA signal is that it depends on the square of the atomic density, and thus the signal is most sensitive to atoms in the dipole trap rather than those in the diffuse cloud of atoms around it, even though there are many more atoms in this cloud. Within the trap it is most sensitive to atoms in the lowest vibrational states of the trap, where the density is highest.

III. SUMMARY OF TRAP LOADING AND EVAPORATION PROCEDURE

The experimental setup and timing sequence are shown in Fig. 3a and Fig. 3b, respectively. Our approach to attaining BEC proceeds as follows: The dipole trap is loaded from a standard Zeeman-slower-fed, six-beam, dark-spot, magneto-optical trap (MOT). This produces, after a loading time of about 8 s, a sample of 7×10^9 ^{23}Na atoms at about 300 K, in a volume of $(2 \text{ mm})^3$. A single, traveling-wave, annular repumping beam, tuned to the $3S\ F=1 \rightarrow 3P_{3/2}\ F=2$ transition, is used along with the cooling light, tuned to the red of the $3S\ F=2$

$! \ 3P_{3=2} F=3$ cycling transition, to form the dark-spot MOT. Nearly all of the atoms are thus in the $F=1$ hyperfine state. This reduces hyperfine-changing collisions in the dipole trap and is required for the application of further cooling techniques. The dipole trap is formed by crossing two focussed beams in the MOT volume, as described below, and is turned on during the final 2.5 seconds of the MOT phase. At this time the intensity of the cooling light is reduced from 6 mW/cm^2 to 3 mW/cm^2 in each beam, producing a weak MOT to further cool the atom sample. Loading the dipole trap directly from the MOT at this point, gives a trapped atom number of only 3×10^4 (measured by absorption imaging 100 ms after the MOT phase).

To increase the number of atoms loaded into the dipole trap a 60 ms transitional "molasses" phase is applied as the MOT is gradually turned off. During this time the magnetic field gradient from the MOT coils is lowered from 0.5 mT/cm to 0 mT/cm and the detuning of the cooling light is increased from 24 MHz to 32 MHz (measured red from the $3S_{1=2} F=2 \rightarrow 3P_{3=2} F=3$ cooling transition at 16973 cm^{-1}). The repumping beam during this period continues to be a single, annular, traveling-wave beam. The ramp starts from a detuned strong MOT condition that at first compresses the atomic cloud. As the ramp continues the temperature of the cloud is decreased. The final temperature of the cloud after this phase is 50 K. The currents in a set of magnetic-field-nulling coils are adjusted in order to achieve the lowest temperature at this phase. After this 60 ms molasses phase all near-resonant laser beams are extinguished by acousto-optical modulators (AOMs), followed by mechanical shutters. This loading process determines the initial phase space density, and thus, whether or not it is finally possible to reach quantum degeneracy.

The molasses phase is followed by a 300 ms period of free evaporation, during which the dipole trapping beams are held at constant power. Finally, we have a period of forced evaporation during which both dipole trapping beams are ramped down in power, simultaneously, over a time of 12.5 s. The timing sequence of the different experimental steps is shown in Fig. 3b. The details of the experiment, and the diagnostics applied to optimize this sequence are discussed in the next section.

IV. EXPERIMENTAL PROCEDURE AND PHOTOASSOCIATION DIAGNOSTICS

The trapping beams are produced by a commercially-bonded fiber laser which can generate up to 100 W of 1.07 μm light. The line width of this laser is 3 nm and the polarization is random. (The polarization changes quickly on the time scale of the typical oscillation periods of the atoms in the dipole trap.) In practice we operate the laser at $\sim 40 \text{ W}$, since it shows excess intensity noise at higher powers. The trapping light passes through one AOM. The first diffracted order from the AOM goes to

the experiment and the intensity of this beam is controlled by the rf-drive power. The beams are divided by a non-polarizing beam-splitter cube and focussed into the vacuum chamber with 300 mm focal length lenses. Note that we do not need to polarize the beams or introduce frequency shifts to wash out interference effects. The angle between the beams inside the chamber is 90° and the beam waist in the crossing region is 61 μm ($1/e^2$ radius). The beam size is obtained from the trap oscillation frequency, laser power, and calculated Stark shift. The plane of the crossed beams is perpendicular to gravity. Each beam has a maximum power of 14 W at the trap location, corresponding to an initial potential depth of $U = k_B T = 510 \text{ K}$ (where k_B is the Boltzmann constant).

To analyze the properties of the atoms in the dipole trap, we can use absorption imaging. The atoms are released from the trap by turning off the trapping laser in order to minimize effects due to ac-Stark shifts caused by the dipole trap. The number and temperature of the atoms are extracted using time-of-flight (TOF) techniques. For short times after the end of the molasses phase, the absorption signal is dominated by the expanding MOT cloud and it is necessary to allow the non-trapped fraction of the atoms to fall away before we can cleanly observe the atoms in the dipole trap. 500 ms after switching off all resonant light we trap 10^7 atoms in the whole dipole potential, and 2×10^6 atoms in the crossed region, with a temperature of 50 K. This results in an initial peak atom density of $9 \times 10^{13} \text{ cm}^{-3}$. The density is derived from the measured temperature, atom number, and trap oscillation frequency, and by assuming that the Gaussian potential can be described by a harmonic approximation at the bottom of the trap.

To measure the trap oscillation frequency we parametrically excite the breathing mode of the trap. First we evaporatively cool the atoms, proceeding 3 s into the usual intensity ramp of the dipole trap (discussed below). We then modulate the power of the dipole trap potential sinusoidally and measure trap loss as a function of modulation frequency using time-of-flight imaging. The mean oscillation frequency of the trap during the free evaporation stage is $1.7 \pm 0.2 \text{ kHz}$. Trap oscillation frequencies for other laser powers are derived from this by scaling to the square root of the measured power in the trap beams. We obtain the trap depth and the waist size from the oscillation frequency and the power in the trapping beams, again making a harmonic approximation [14].

To probe the evolution of the atom cloud during the molasses and evaporation stages, we employ a new technique which allows us to directly monitor the density of the atoms inside the trap. The density is probed by a PA laser which resonantly produces bound excited state molecules (in the $J = 0$ rotational level of the 0_g component of a vibrational level in the $(1)^3 g^+$ ($S + P_{3=2}$) potential [15]). The laser frequency for this transition is 16845.16 cm^{-1} . The molecules which are formed are then excited by an additional laser (at 17099.95 cm^{-1}) to an autoionizing level (see Fig. 2). The ions that are

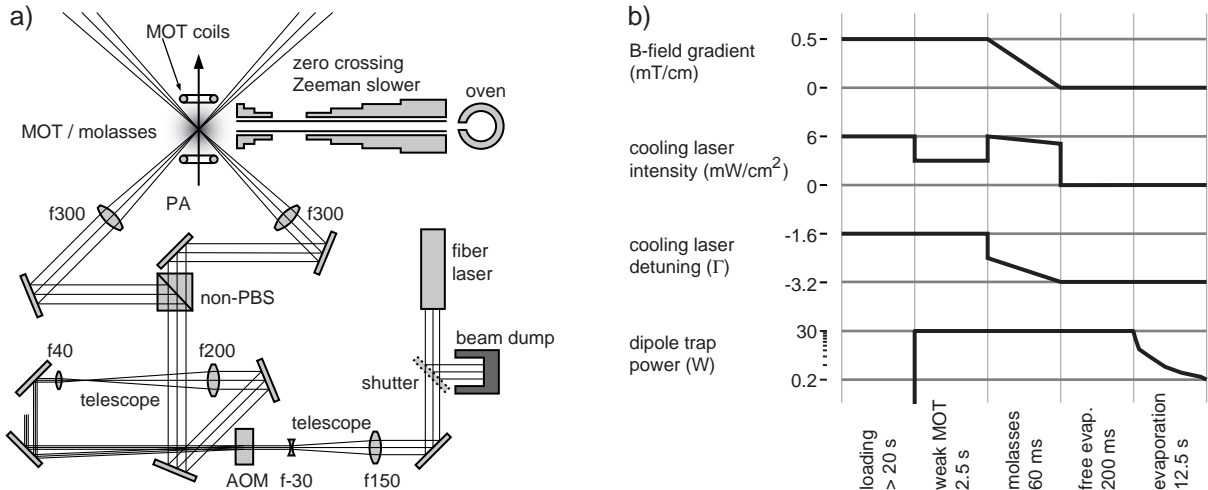


FIG. 3: a) Sketch of the experimental setup. b) Tuning sequence of the experiment indicating the MOT magnetic field gradient, MOT/cooling laser detuning and intensity, and the total power in the dipole trap beam s. There are four stages to the loading of the trap. A strong MOT period is used for rapid loading. The weak MOT period then reduces the temperature of the MOT. These are followed by an optimized ram-ped-molasses phase, and a free evaporation phase, where the intensity of the dipole laser is held constant. Finally, there is a forced evaporation phase where the intensity of the dipole laser is successively reduced.

produced are then efficiently detected by a microchannel plate. This ion signal is proportional to the volume integral over n^2 , where n indicates the atom density. At the temperatures under consideration here, this s-wave PA transition is in the Wigner Law regime and the PA signal is not directly dependent on the temperature (average collision energy) of the atoms, but simply depends on the density (as discussed in [10]).

In sodium the molecular energy levels are such that in a MOT a steady ion signal is produced by the trapping beams themselves, so it is necessary to turn them off to see the PA signal. The PA and ionizing lasers are then turned on (4 mW and 5 mW, respectively, in an approximately 100 μm spot size). The ion signal that is produced can be used to optimize the cooling process and the loading into the trap. Figure 4 shows the ion signal, measured in this way (integrated over a 10 ms period), during our optimized 60 ms molasses ramp. The density increases continuously until the end of the 60 ms, at which point the magnetic field is zero. During the last few milliseconds of this stage the magnetic field at the location of the dipole trap is so small that the conditions are characteristic of a true optical molasses, and the final temperature is not improved by extending the molasses period beyond the end of the magnetic field ramp.

After the molasses phase we turn off all of the cooling light beams and wait before starting the forced evaporation ramp. The evolution of the density during this first 300 ms free evaporation period helps to reach the extremely high phase space density needed for a successful forced evaporation.

During the free evaporation phase (where the dipole laser power is held constant), we can again probe the time evolution of the density of the atoms in the trap by

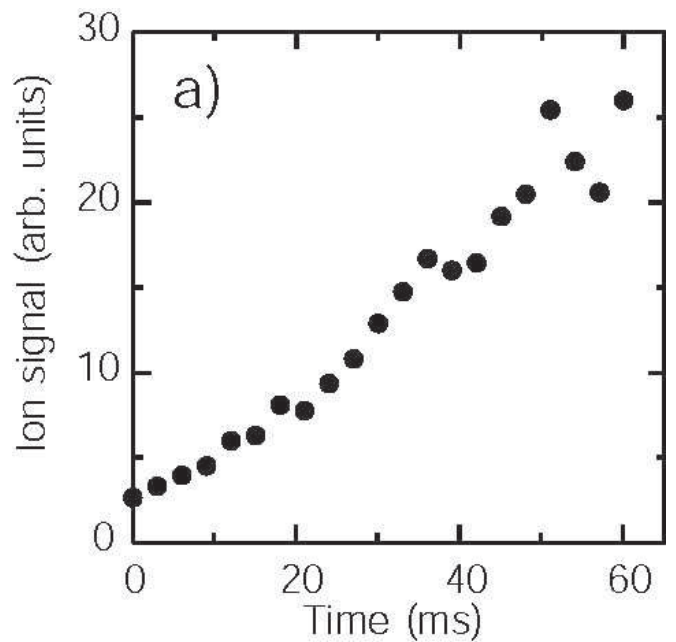


FIG. 4: The Na_2^+ ion signal due to photoassociation (PA), as explained in the text, which is used to optimize the trap loading sequence. The MOT laser tuning is shifted and the magnetic field ramp down over 60 ms. This scan shows the resulting ion signal when the ramping has been optimized.

using our PA technique. We are continuously producing and ionizing molecules during this time, however, a 1 s duration PA pulse (at a power of 340 W) reduces the atom number by only 5% and represents a small perturbation on the trapped atom density dynamics. In Fig. 5

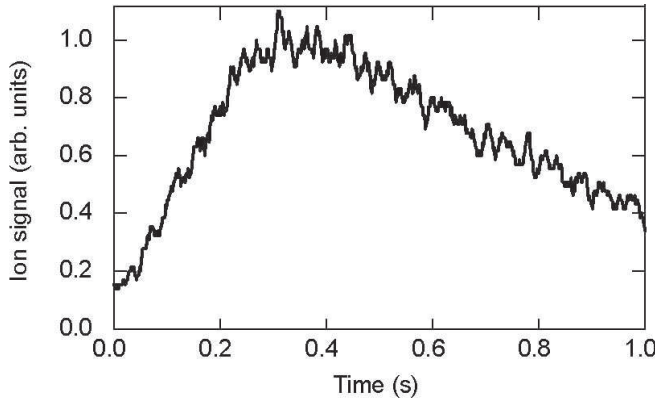


FIG. 5: Ion signal during the first one second of evaporation with constant trap intensity. During this stage all additional cooling light is turned off and the PA and ionizing laser powers are lower than in Fig. 4. The ion signal (integrated for 10 ms periods) indicates the density evolution during this free evaporation stage. The density increases during this phase while atoms are lost, which indicates that during this time the atomic cloud is rapidly cooling.

the ion signal shows that the density begins to increase during this trap holding phase. The evaporation process causes atom loss and is not compensated by any loading during this time. The remaining atoms rethermalize at higher density. The increase in density slows down with time and, finally, if held too long, the loss out of the trap becomes the dominant process and the density starts to decrease. This can be seen for times later than about 300 ms in Fig. 5. The trap lifetime under these conditions, as seen in the figure, is fairly short and is possibly limited by beam-pointing instabilities induced by thermal effects (due to the high RF power in the AOM which controls the power into the trapping beam). Under other conditions longer lifetimes are obtained, as discussed below.

The initial phase space density in the trap, just 500 ms after the molasses phase (or 200 ms after the free evaporation phase), is 1×10^{20} . Using the corresponding value for the density and the three-body rate constant from [16] ($K_3 = 1.1 \times 10^{30} \text{ cm}^6 \text{ s}^{-1}$, measured for the $F=1$, $m_F = -1$ state, with a density of 10^{14} cm^{-3}), we can infer the three-body loss rate in our trap to be 0.01 s^{-1} . It is thus possible that the three-body losses contribute to limiting the density achievable by free evaporation. The estimated elastic collision rate is initially 2 kHz . During the optimized loading ramp and after free evaporation the density increases by about a factor of 300, from 3×10^{11} in the MOT, to $9 \times 10^{13} \text{ cm}^{-3}$ in the dipole trap.

At the time when free evaporation gives the maximum density we start a period of forced evaporation by simply lowering the power simultaneously in both dipole trap beams. The most energetic atoms escape and the remaining atoms rethermalize at a lower temperature with a higher phase space density. The rethermalization rate

given by the elastic collisions slows down as the trap potential (and therefore the oscillation frequency) is lowered. At the end of our evaporation ramp we calculate a factor of 25 lower collision rate than at the beginning. Our ramp is divided into 7 segments during each of which the intensity is dropped, approximately linearly, by a factor of two (see Fig. 6b). (The ramp function fed to the electronics is linear, however, nonlinearities in the rfdrive electronics and the AOM response lead to some curvature in the actual ramp segments, which are not corrected for.) The duration of each segment is optimized experimentally to give the largest phase space density. The temperature at the end of each segment is determined by the trap depth at the end of that segment. Our ramp is 12.5 s long and approximately follows the theoretically optimized curve $U(t) / 1 = (1 + t^{\alpha})^{-1}$ with $\alpha = 3.5$ $s = 3.5$, as derived in Ref. [17].

Figure 6 shows the decrease of the atom number and temperature with the lowering of the trap oscillation frequency. The temperature decreases monotonically, roughly as a constant fraction 0.1 of the potential depth [17]. Figure 7 shows the evolution of the peak density, derived from the data in Fig. 6 and assuming a harmonic potential. Once BEC begins we fit the atom distribution to a sum of two components: a broad thermal distribution and a narrow distribution representing the condensate fraction. The temperature is extracted from the fit to the thermal fraction and the peak density from a sum of the densities of the thermal and the condensed components. The density decreases at first, due to the loss of atoms and the decreasing confinement as the trap is weakened. The density then rises as the condensate starts to form. As the intensity, and thus the trap frequency, is lowered, the temperature also decreases, as shown in Fig. 6. Taking all the parameters into account one sees that the resulting phase space density increases as the evaporation proceeds, as seen in Fig. 7. The speed of this increase is sensitive to the initial conditions. At the lowest trap frequencies most of the atoms are already condensed and the density and phase space densities begin to go down as the trap potential is further expanded. At the end of the 12.5 s intensity ramp we observe a condensate with a typical number of 1.5×10^5 atoms, or about 80% of the atoms. The final trap depth is 2.9 K and the oscillation frequency is 120 Hz with 80 mW of power in each trapping beam. The peak density is $9 \times 10^{13} \text{ cm}^{-3}$, and the observed condensate lifetime is 18 s. Most likely this lifetime is limited by noise on the trapping potential. The background gas pressure is $4 \times 10^{-9} \text{ Pa}$ ($3 \times 10^{-11} \text{ torr}$), measured by an ionization gauge.

A straightforward investigation of the onset of BEC can be made by probing the atoms on a photoassociation transition and measuring the PA rate by either the ion signal, as discussed above, or the loss of the atoms out of the trap, as shown in Fig. 8. Here the PA laser intensity is much higher than in Fig. 5. We can observe the onset of BEC using the PA technique as it detects the steep rise in

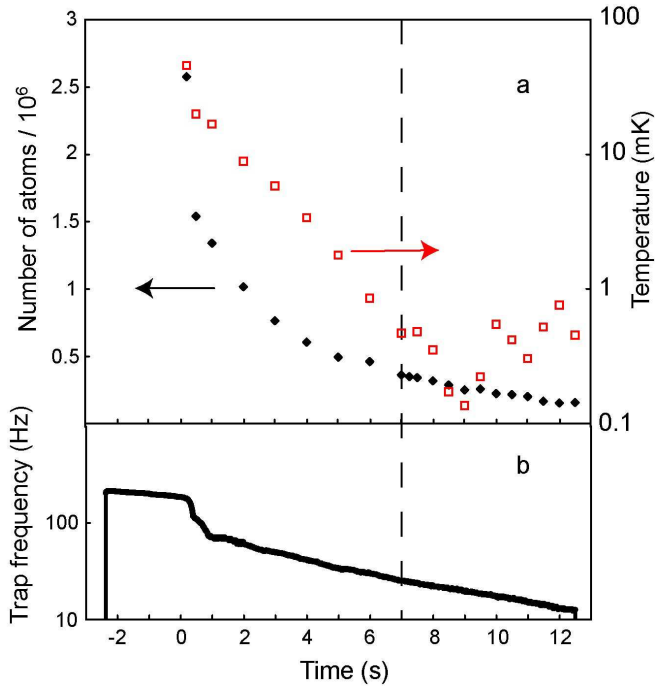


FIG . 6: (Color online) a) The evolution of the temperature of the thermal fraction (squares) and the trapped atom number (diamonds) during the evaporation ramp p. The temperature of the thermal fraction changes linearly with the potential depth until approximately the point where a condensate starts to form. The zero of time is the beginning of the forced evaporation ramp p, after 300 ms of free evaporation with a static trap depth. b) The evaporation ramp p (on a log scale) of the trap frequency versus time. The dashed vertical line indicates the time of the onset of BEC .

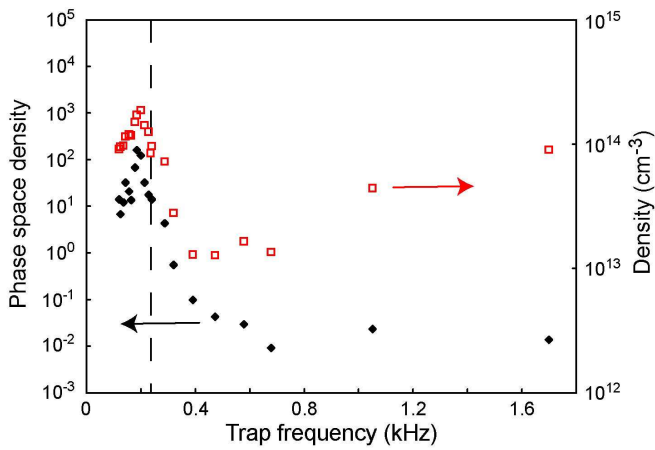


FIG . 7: (Color online) Density evolution in the trap during the forced evaporation ramp p (squares, right vertical axis) as a function of trap oscillation frequency. The peak phase space density as a function of the trap oscillation frequency (diamonds, left vertical axis). The dashed vertical line indicates the onset of BEC and to the right of this line the condensate fraction is less than 1 % .

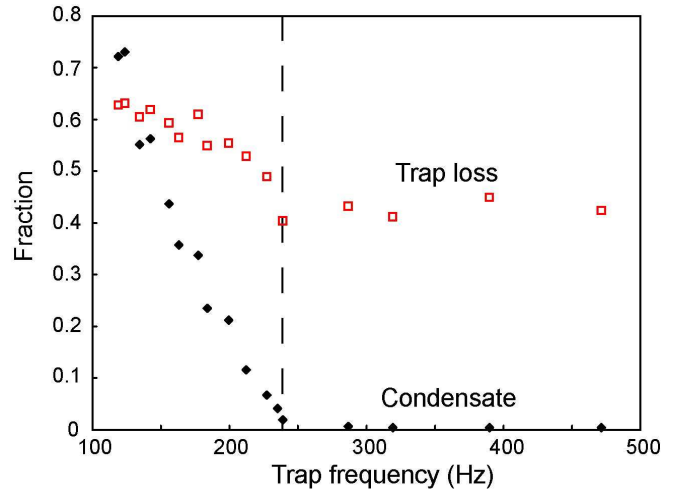


FIG . 8: (Color online) Condensate fraction of the trapped atoms (diamonds) and fractional trap loss due to a 10 ms, on-resonance photoassociation pulse, as explained in the text (squares), as functions of the trap oscillation frequency. The dashed vertical line indicates the onset of BEC .

density that accompanies the phase transition. PA trap loss measurements sometimes result in higher signal-to-noise than the ion signal discussed above, and can also be used for such measurements, albeit destructively.

Measurements of the fractional trap loss are shown in Fig. 8 and are produced by illuminating the trap with a laser resonant with the PA transition discussed above. The cloud is illuminated for a time of 10 ms and contains 4 mW in a 100 μm spot. The remaining atom number is compared with the atom number when the PA beam is tuned off resonance to give the fractional trap loss measurements plotted in the figure. Near the end of the evaporation ramp the trap depth is only 2.9 K and the probe beam, which is detuned red from the atomic resonance, significantly distorts the trap potential by inducing an additional dipole force on the atoms. To prevent this effect a laser, blue detuned from the resonance (5 mW), is added to counteract this dipole force. Fig. 8 shows that when the condensate emerges the fractional trap loss increases rapidly and can serve as an indicator of the presence of the condensate.

To understand Fig. 8 in more detail it is essential to know which parts of the atomic distribution are contributing to the PA signal. Figure 9 shows line profiles of time-of-flight pictures of the atom distribution, taken with and without the PA beam applied (with the same intensity and duration as above). Figure 9a was taken when there was only a thermal cloud present, and Fig. 9b was taken after the appearance of a condensed fraction within the thermal cloud. The upper profile in both of the plots show the profile when the PA beam was applied but tuned off-resonance, while the lower profiles show which atoms remain after the PA beam tuned to resonance was applied. In both cases one sees that after the PA pulse a large fraction of the coldest atoms are

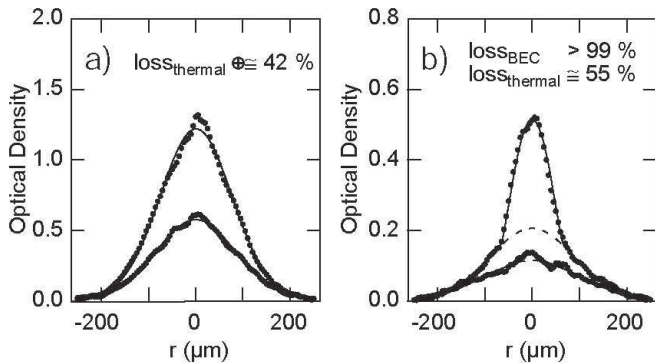


FIG. 9: Line profiles taken from time-of-flight pictures of an atomic ensemble. The upper traces are taken with the photoassociation (PA) beam tuned off resonance and the lower profiles after applying the PA beam on resonance. These profiles are produced by finding the center of a time-of-flight picture of an atom cloud and azimuthally averaging over 180° . The two independent half-circles of data, one used for negative r , allow for better signal-to-noise, while the asymmetry in r permits its some judgment of the noise level. a) Time-of-flight profiles with a thermal kinetic energy distribution and t. b) Time-of-flight profiles of an atomic ensemble with an initial condensed fraction of 41%. The lines through the data are two-component (thermal/BEC) fits to the data. The dashed lines show the thermal contribution.

missing. This is because the coldest atoms are mostly held near the trap center, where the density is highest. When a fraction of the atoms are condensed, as in Fig. 9b, the condensed part contributes the most to the PA signal because this part of the atomic distribution has the highest density – even though the PA rate coefficient for a condensate is lower by a factor of two than that of a thermal ensemble [10, 18].

V. DISCUSSION

As shown in Fig. 1 we can quite easily create a number of condensates by recycling the trap beams, as long as the crossing regions stay within the volume of the MOT. The trapping beams are brought into the chamber through 300 mm lenses and are diverging as they exit the vacuum chamber. Each exiting beam is then recolimated by another 300 mm lens, and retroreflected back through the same lens on a small angle, to intersect the orthogonally-propagating beams. This simple construction can produce an array of four traps. Such an array of condensates immediately suggests that one might use them in a variety of atom-optics experiments. One can, for instance, imagine launching one condensate into another by scanning the retroreflecting mirror. With more sophisticated optics one can think of creating a regular lattice array of condensates in three dimensions, with spacings on a scale of about 100 μm .

Optical traps can produce spinor condensates, as demonstrated in Ref. [3]. By applying a magnetic field

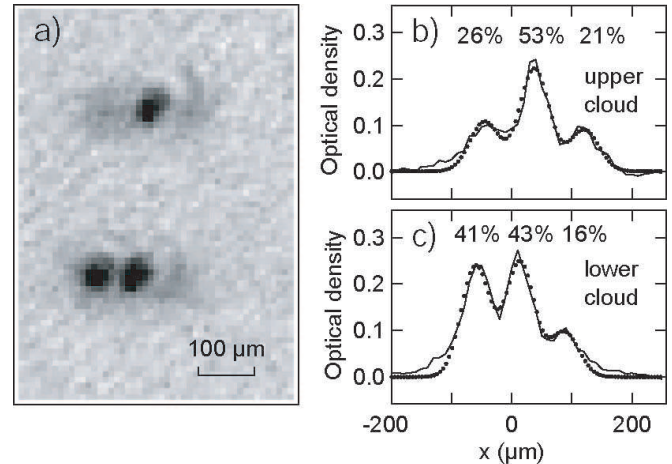


FIG. 10: a) Absorption images after a time-of-flight of two condensates generated by retroreflecting one trapping beam as described in the text. During the time-of-flight a magnetic field gradient is applied, separating the m_F levels. Line trace of the distribution of atoms between the $m_F = 0, \pm 1$ states for the upper (b), and lower (c) cloud. The distribution depends on the position of the trap in the MOT. The dotted lines represent a fit to the sum of three displaced Gaussians, from which the relative populations are extracted.

gradient during time-of-flight one can separate and observe the different magnetic spin components. We can also create a mixture between the three available spin states, $m_F = 0, \pm 1$. In Fig. 10 we have recycled and refocused only one of the trapping beams to generate two traps. By applying the same evaporation ramp to all of the beams we generate two condensates at the same time. We then apply a magnetic field gradient with our MOT coils and, in this case, we find that the population of the magnetic spin components is different for the two traps. In fact, the spin distributions map to the different trap positions and allows for almost pure spin states under some conditions. By successively changing the crossing position and having a little bit luck, one is able to obtain most of the population in a single magnetic sublevel without having to apply any additional optical pumping. The polarization of the sample is apparently due to the local magnetic field and laser imbalances in the MOT and molasses phases, which produce varying m_F distributions in different spatial locations, which are then preserved in the trap.

The technique that we describe here represents our first effort and could be improved upon by, amongst other things, stabilizing the laser intensity at higher powers with an AOM. Problems due to pointing instabilities could also be improved by better heat-sinking of the AOM to reduce temperature fluctuations caused by changes in rf powers to the AOM. The beam spot size has not been optimized in these experiments, and it is still to be determined if we can trap more atoms and produce larger condensates by using a larger spot size (taking advantage of the factor of 2–3 more power that

we have available). Eventually, at large trap sizes the evaporation to BEC will be stalled by the lack of density or limited by background gas scattering as we require longer evaporation times.

In this paper we have demonstrated a straightforward, all-optical method of production of sodium Bose-Einstein condensates. With some variation in parameters, this approach could be used for other species as well. In addition, we have introduced a new technique for probing the density evolution in the dipole trap during the evaporation process using photoassociation. This tool enables us to optimize the production of a Bose-Einstein condensate

in a simple manner. Under some conditions it also allows for non-destructive monitoring of the condensate evolution. The fixed-focus crossed-dipole trap technique is capable of generating multiple condensates simultaneously, which can be connected with each other via the dipole trap beams. The simple optical system allows for a great deal of flexibility in constructing experiments, and also provides good optical access to the system. The ability to produce multiple independent condensates suggests a number of interesting atom optics experiments where, for instance, one could collide or channel condensates in the waveguides provided by the trapping beams.

[1] C. Adams, H. J. Lee, N. Davidson, M. Kasevich, and S. Chu, *Phys. Rev. Lett.* **74**, 3577 (1995).

[2] K. Davis, M. O. Mewes, M. R. Andrews, N. J. van Duyne, D. S. Durfee, D. M. Kurn, and W. Ketterle, *Phys. Rev. Lett.* **75**, 3969 (1995).

[3] M. D. Barrett, J. A. Sauer, and M. Chapman, *Phys. Rev. Lett.* **87**, 010404 (2001).

[4] T. Wöber, J. Herbig, M. Mark, H.-C. Nagerl, and R. Grimm, *Science* **299**, 232 (2003).

[5] A. Griesmaier, W. J., H. S., J. Stuhler, and T. Pfau, *Phys. Rev. Lett.* **94**, 160401 (2005).

[6] Y. Takasu, K. Maki, K. Komori, T. Takano, K. Honda, M. Kumakura, T. Yabuzaki, and Y. Takahashi, *Phys. Rev. Lett.* **91**, 040404 (2003).

[7] S. R. Granade, M. E. Gehm, K. M. O'Hara, and J. E. Thomas, *Phys. Rev. Lett.* **88**, 120405 (2002).

[8] S. J. M. Kuppens, K. L. Corwin, K. W. M. Iller, T. Chupp, and C. E. Wieman, *Phys. Rev. A* **62**, 013406 (2000).

[9] J. Weiner, V. S. Bagnato, S. Zilio, and P. S. Julienne, *Reviews of Modern Physics* **71**, 1 (1999).

[10] K. Jones, E. Tiesinga, P. D. Lett, and P. S. Julienne, *Reviews of Modern Physics* under review (2006).

[11] P. Courteille, R. S. Freeland, H. D. J., F. A. van Abeelen, and B. J. Verhaar, *Phys. Rev. Lett.* **81**, 69 (1998).

[12] F. K. Fathemi, K. M. Jones, and P. D. Lett, *Phys. Rev. Lett.* **85**, 4462 (2000).

[13] L. E. E. de Araujo, J. D. W. Einstein, S. D. Gensemer, F. K. Fathemi, K. M. Jones, P. D. Lett, and E. Tiesinga, *J. Chem. Phys.* **119**, 2062 (2003).

[14] S. Friebel, R. Scheunemann, J. Walz, T. Hansch, and M. Weitz, *Appl. Phys. B* **67**, 699 (1998).

[15] K. Xu, Y. Liu, J. Abo-Shaeer, T. Mukaiyama, J. Chin, D. Miller, W. Ketterle, K. M. Jones, and E. Tiesinga, *Phys. Rev. A* p. accepted for publication (2005).

[16] D. M. Stammer-Kurn, M. Andrews, A. P. Chikkatur, S. Inouye, H. J. Miesner, J. Stenger, and W. Ketterle, *Phys. Rev. Lett.* **80**, 2027 (1998).

[17] K. M. O'Hara, M. E. Gehm, S. R. Granade, and J. E. Thomas, *Phys. Rev. A* **64**, 051403(R) (2001).

[18] D. Harber, H. Lewandowski, J. M. Gwirik, and E. Cornell, *Phys. Rev. A* **66**, 053616 (2002).